Smart Fault Detection of Reciprocating Air Compressors Based on Electrical Signature Analysis

Armin Toroghi
School of Mechanical Engineering
University of Tehran
Tehran, Iran
armintoroghi@ut.ac.ir

Ali Sadighi
School of Mechanical Engineering
University of Tehran
Tehran, Iran
asadighi@ut.ac.ir

Abstract*— Air compressors are one of the most common industrial devices and their functionality is vital for many industries. Therefore, providing an accurate and cost-effective strategy for monitoring their condition is crucial. In this paper, a fault detection approach based on Electrical Signature Analysis (ESA) is proposed. Firstly, the theoretical rationale of using electrical signals for diagnosing mechanical faults is discussed by simulating a model of an electrically-driven air compressor and demonstrating the electromechanical coupling between compressor sub-systems. Next, a fault detection approach based on ESA is elucidated that consists of measuring the voltage and current signals of the compressor, feature extraction from the signals, and classification of the features using machine learning algorithms. Implementation of the approach on experimental data resulted in the accurate detection of mechanical faults.

Keywords—Reciprocating Air Compressor, Condition Monitoring, Fault Detection, Electrical Signature Analysis, Machine Learning

I. INTRODUCTION

Air compressors are widely used in various industries to increase the air pressure that pneumatic systems require to operate. Several types and configurations have been proposed and designed for the compressors, among which reciprocating air compressors are one of the most conventional ones. Given this widespread usage and their important duty, ensuring their health and functionality is crucial to many plants, and the development of methods to monitor their performance has been the subject of several studies. Townsend et al. [1] have proposed a condition monitoring approach for electrically-driven reciprocating air compressors used in the oil industry by monitoring the temperature of the connecting rods. A cost analysis is also conducted that shows a significant cut in the operating cost can be obtained using the proposed approach. A more recent study conducted by the same team examines the feasibility of continuous monitoring of the cylinder pressure for reciprocating compressors. The results of this research showed an increased cost-efficiency and monitoring accuracy could be obtained by the pressure monitoring approach. A notable amount of previous research in the field of fault diagnosis of the compressors has been focused on using vibratory signals to monitor the performance of the system. Pichler et al. [2] used the change introduced to the time-frequency representation of vibration data acquired from the compressor to detect compressor faults. In [3] a semi-supervised condition monitoring approach was proposed for reciprocating refrigeration compressors based on vibration analysis. The semi-supervised approach addresses the difficulty of labeling the acquired data and obtaining prior class definitions.

However, using vibration analysis for detecting faults of rotary machines has been reproved for requiring high-cost sensors and the difficulty and complexity of installation in some applications [4][5]. Electrical motors are among the most conventional types of compressor drives. A powerful alternative to the vibration analysis is an approach called '*Electrical Signature Analysis*'(ESA) that was first introduced to detect mechanical faults of induction motors [6]. In this method, electrical signals, e.g. voltage, current, and power or features calculated from them are considered to track and detect faults in the system. Application of this method is not confined to induction motors and several studies have proven it to be successful in detecting faults and anomalies in different mechanical systems. Shahriar et al. [7] utilized the ESA method for diagnosing defects occurring in an external drivetrain bearing of a wind turbine. Popaleny et al. [8] studied the effect of both mechanical and electrical faults on the current spectrum of electrical submersible pumps. The installation of sensors on these pumps is not feasible, but using the ESA approach, the condition monitoring could be performed remotely on these devices. Efforts have also been made to implement the approach to reciprocating compressors. Gu et al. [9] transformed the current signals obtained from an electrically-driven compressor using modified bispectrum transform and utilized them to detect valve faults.

In this paper, first of all, a model of the electrically driven air compressor will be presented and used for simulation. Next, a fault detection scheme using features extracted from the electrical signals will be inaugurated. After that, the simulation results of the effects of four common mechanical faults on the electrical signals will be shown as a proof of concept, and finally, results of implementing the proposed fault detection approach on the obtained experimental data will be presented.

II. MATHEMATICAL MODEL OF THE SYSTEM

An electrically-driven air compressor consists of two sub-systems, i.e. the electrical sub-system and the mechanical sub-system. The mainstay of the idea of using the ESA approach in detecting air compressor faults is the electromechanical coupling that exists between the sub-systems. The electrical sub-system is in charge of creating the electromagnetic torque that drives the motor shaft with a rotational speed. The motor shaft is connected to the mechanical sub-system, either directly or using a belt and pulley, and provides the rotational movement of the

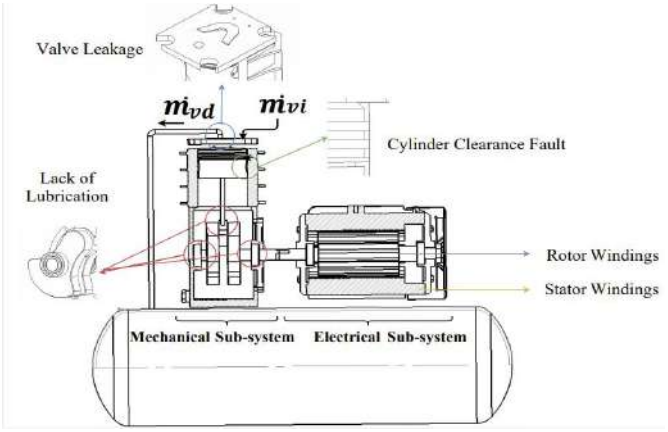

Fig. 1. Electrically-driven compressor and location of the studied faults

compressor crankshaft. The crankshaft is connected to a connecting rod that transforms the rotational movement of the crankshaft to the linear movement of the piston inside the cylinder, which increases the pressure of the air. The physical connection between the two sub-systems might provide an intuitive deduction that faults in the mechanical sub-system will show their footprint on the electrical system and thus, the electrical signatures. However, in order to provide a strong proof of concept for the idea of using the ESA for detecting mechanical faults of the compressor, an outright analytical modeling of the compressor sub-systems followed by a simulation is presented in this section.

A. Electrical Sub-system

Single-phase induction motors with rotors fabricated in the squirrel cage style and with permanent capacitors are the most common type of drives used for low-power compressors, as the one studied in this research. Since the objective of this modeling is only proving the concept of electromechanical coupling between the compressor sub-sections, without any loss of generality, we can only consider this type of drive for the electrical sub-section.

In the modeling of single-phase motors, it is common to model the auxiliary and main windings of the stator in two phases. The rotor is also often considered and modeled in two-phase style. The relation between current and flux linkage could be written as[10]:

$$\begin{bmatrix} \lambda_{main} \\ \lambda_{aux} \\ \lambda_1 \\ \lambda_2 \end{bmatrix} = L \begin{bmatrix} i_{main} \\ i_{aux} \\ i_1 \\ i_2 \end{bmatrix} \tag{1}$$

In which i denotes current, λ denotes flux linkage, subscripts $main$ and aux refer to the main and auxiliary windings of the stator and 1 and 2 refer to the two considered phases for the rotor, and:

$$L = \begin{bmatrix} L_{main} & 0 & L_{main,1}(\theta) & L_{main,2}(\theta) \\ 0 & L_{aux} & L_{aux,1}(\theta) & L_{aux,2}(\theta) \\ L_{main,1}(\theta) & L_{aux,1}(\theta) & L_r & 0 \\ L_{main,2}(\theta) & L_{aux,2}(\theta) & 0 & L_r \end{bmatrix} \tag{2}$$

In which L with single subscript denotes self-inductance and with two subscripts denotes the mutual inductance between the windings identified by the subscripts. Considering the equivalent circuit of the induction motor, voltage relations could be written as[11]:

$$v_{main} = i_{main} R_{main} + \frac{d\lambda_{main}}{dt} \tag{3}$$

$$v_{aux} = i_{aux} R_{aux} + \frac{d\lambda_{aux}}{dt} \tag{4}$$

$$v_1 = 0 = i_1 R_r + \frac{d\lambda_{r1}}{dt} \tag{5}$$

$$v_2 = 0 = i_2 R_r + \frac{d\lambda_{r2}}{dt} \tag{6}$$

In which v denotes voltage and R is the resistance of the winding indicated by the subscript and the subscript r refers to the rotor. By taking derivation from the co-energy relation of the motor with respect to the rotor angle, θ_m, the created electromagnetic torque, T_e is given by:

$$\begin{aligned} T_e = i_{main}\, i_{r1} \frac{dL_{main,r1}(\theta_m)}{d\theta_m} + i_{main}\, i_{r2} \frac{dL_{main,r2}(\theta_m)}{d\theta_m} \\ + i_{aux}\, i_{r1} \frac{dL_{aux,r1}(\theta_m)}{d\theta_m} + i_{aux}\, i_{r2} \frac{dL_{main,r2}(\theta_m)}{d\theta_m} = \\ \left(\frac{poles}{2}\right)[-L_{main,r}(i_{main}\, i_{r1} \sin\theta_m + i_{main} i_{r2} \cos\theta_m) + \\ L_{aux,r}(i_{aux} i_{r1} \cos\theta_m - i_{aux} i_{r2} \sin\theta_m)] \end{aligned} \tag{7}$$

By writing the current and voltage relations of the stator for the steady-state condition and eliminating the rotor current from the equations, the phasor form of the relation between current and flux linkage of the stator windings could be written as:

$$\begin{aligned} \hat{\lambda}_{main} = [L_{main} - jL_{main,r}^2(\hat{K}^+ + \hat{K}^-)]\hat{I}_{main} \\ + L_{main,r} L_{aux,r}(\hat{K}^+ - \hat{K}^-)\hat{I}_{aux} \end{aligned} \tag{8}$$

$$\begin{aligned} \hat{\lambda}_{aux} = -L_{main,r} L_{aux,r}(\hat{K}^+ - \hat{K}^-)\hat{I}_{main} \\ + [L_{aux} - jL_{aux,r}^2(\hat{K}^+ + \hat{K}^-)]\hat{I}_{aux} \end{aligned} \tag{9}$$

In which the $\hat{}$ superscript is used to show the phasor form, and we have :

$$\hat{K}^+ = \frac{s\omega_e}{2(R_r + js\omega_e L_r)} \tag{10}$$

$$\hat{K}^- = \frac{(2-s)\omega_e}{2(R_r + j(2-s)\omega_e L_r)} \tag{11}$$

In these equations, s is the rotor slip that can be calculated as:

$$s = \frac{\omega_e - \omega_m}{\omega_e} \tag{12}$$

where ω_e is the electrical frequency and ω_m is the mechanical speed of the rotor. Contemplating (2), (3), (8) and (9), $\hat{I}_{main}$ and $\hat{I}_{aux}$ could be calculated as:

$$\begin{bmatrix} R_{main} + j\omega_e[L_{main} - jL_{main,r}^2(\hat{K}^+ + \hat{K}^-)] \\ -j\omega_e[L_{main,r} L_{aux,r}(\hat{K}^+ - \hat{K}^-)] \\ j\omega_e[L_{main,r} L_{aux,r}(\hat{K}^+ - \hat{K}^-)] \\ R_{aux} + jX_c + j\omega_e[L_{aux} - jL_{aux,r}^2(\hat{K}^+ + \hat{K}^-)] \end{bmatrix} \begin{bmatrix} \hat{I}_{main} \\ \hat{I}_{aux} \end{bmatrix} = \begin{bmatrix} V_c \\ -V_c \end{bmatrix} \tag{13}$$

The total current passing the electrical terminal can be calculated by inverting the matrix of coefficients in (5). Equation (13) shows that a change in mechanical shaft speed affects the terminal current by changing slip. The relationship between the rate of change in the shaft speed and the torques applied to the shaft could be obtained by considering Newton's 2nd law:

$$J\frac{d\omega_m}{dt} = T_e - T_l \quad (14)$$

In which J denotes the moment of inertia and T_l is the load torque. Therefore, if the load torque is changed by the occurrence of a fault in the mechanical sub-system, its effect could be traced by viewing the change introduced in the electrical sub-system signals.

B. Mechanical Sub-system

In order to obtain the mathematical model of the mechanical sub-system, equations of the thermodynamic processes, and dynamic equations of motion are written. In these equations, subscript c refers to the cylinder and subscripts i and d refer to inlet and discharge respectively. First, the air that is inside the compressor cylinder is considered as a control volume (CV) and the first law of thermodynamics is applied to it [12]:

$$\dot{Q} - \dot{W}_s - \dot{W}_p = \frac{\partial(E_{cv})}{\partial t} + \dot{m}_{out}(h_d)_{out} - \dot{m}_{in}(h_i)_{in} \quad (15)$$

In which $\dot{Q}$ is the rate of the heat applied to the CV, E_{cv} is the internal energy of the CV, $\dot{m}$ is the rate of mass that is either entering or leaving the CV that is shown by its subscript. This equation could be simplified by the assumption that the specific kinetic and potential energies from the inlet to the outlet of the CV remain constant. Also, no external shaft work, $\dot{W}_s$, is considered to influence the CV and the thermodynamic processes are deemed to be reversible and adiabatic. Due to the small pressure drops occurring in the system, the Mach number of the fluid is small and the flow is incompressible. $\dot{W}_p$, the rate of work that changes the shape of the CV is:

$$\dot{W}_p = P_c\dot{V}_c \quad (16)$$

Also, the discharge and inlet enthalpies can be obtained as:

$$h_d = h_c = \frac{{c_c}^2}{\gamma - 1} \quad (17)$$

$$h_i = \frac{{c_i}^2}{\gamma - 1} \quad (18)$$

In which C is the speed of sound and γ is the ratio of the specific heats. Here, we assume that no leakage exists from the CV. $\dot{P}_c$, the pressure change relation can be obtained as:

$$\dot{P}_c = \frac{1}{V_c}\{{c_i}^2\dot{m}_{vi} - {c_c}^2\dot{m}_{vd} - \gamma P_c\dot{V}_c\} \quad (19)$$

and V denotes volume. By considering kinematics of the compressor, we obtain v_θ the piston velocity and a_θ acceleration:

$$v_\theta = R_1\omega\left[sin\theta_c + \frac{R_1}{2R_2}sin2\theta_c\right] \quad (20)$$

$$a_\theta = R_1\omega^2\left[cos\theta_c + \frac{R_1 cos2\theta_c}{R_2}\right] \quad (21)$$

Where ω is the crankshaft speed, θ_c is the crank angle, R_1 is the crank radius and R_2 the length of the connecting rod. The volume of the CV is calculated as:

$$V = A\{l_c + R_1(1 - cos\theta_c) + R_2(1 - cos\emptyset_c)\} \quad (22)$$

In which A is the cross-sectional area of the piston, l_c the cylinder clearance and $\emptyset_c$ is the connecting rod angle. Considering the geometric relations between parts of the compressor and taking the time derivative of equation (22) we have:

$$\dot{V} = AR_1\omega sin\theta_c + \left\{\frac{\frac{R_1}{R_2}cos\theta_c}{\sqrt{1-(\frac{R_1}{R_2}sin\theta_c)^2}}\right\} \quad (23)$$

For calculating the mass flow rate of air through the discharge valve, $\dot{m}_{vd}$, the equation of incompressible flow through an orifice gives:

$$\dot{m}_{vd} = sign(P_c - P_d^e)C_{dd}(x)A_{fd}\sqrt{2\rho_c|P_c - P_d^e|} \quad (24)$$

Where P_d^e is the effective pressure in the discharge plenum, $C_{dd}(x)$ the coefficient of discharge as a function of the valve position, and A_{fd} the valve slot area. A similar relation also exists for the inlet valve. The equation of changes in T, temperature, and ρ, density during an isentropic process is calculated as:

$$T_2 = T_1(\frac{P_2}{P_1})^{\frac{\gamma-1}{\gamma}} \quad (25)$$

$$\rho_2 = \rho_1(\frac{P_2}{P_1})^{\frac{1}{\gamma}} \quad (26)$$

And the speed of sound is calculated as:

$$c = \sqrt{\gamma RT} \quad (27)$$

Now, f_p, the force created by the pressure inside the CV and the inertial force created by the moving parts of the compressor, f_m, that are tangential to the crankshaft are calculated as:

$$f_p = P_cA_c\left(sin\theta_c + cos\theta_c\frac{\left(\frac{R_1}{R_2}\right)sin\theta_c}{\sqrt{1-\left(\frac{R_1}{R_2}\right)^2sin^2\theta_c}}\right) \quad (28)$$

$$f_m = m_{rec}\ddot{x}_p\left(sin\theta_c + cos\theta_c\frac{\left(\frac{R_1}{R_2}\right)sin\theta_c}{\sqrt{1-\left(\frac{R_1}{R_2}\right)^2sin^2\theta_c}}\right) \quad (29)$$

Where m_{rec} is the mass of reciprocating parts and $\ddot{x}_p$ the piston acceleration. T_p, the torque exerted on the crankshaft that is created from the gas pressure is calculated as:

$$T_p = r(f_p + f_m) \quad (30)$$

Finally, the load torque is obtained as:

$$T_l = T_p + T_f \quad (31)$$

III. Simulation of the Electromechanical Coupling

In order to investigate the electromechanical coupling and to manifest the effect of mechanical faults on the electrical signatures, a simulation of the system is conducted. The simulation was conducted in MATLAB/SIMULINK using the set of equations presented in the previous sections. Cylinder pressure values obtained from the simulation during a

complete cycle are shown in Fig. 2. In this research, four types of compressor faults are studied in simulation and the experiment: Valve leakage, lack of lubrication, tank leakage, and excessive piston-cylinder clearance.

A leaking valve will lead to an increased area for the air to escape from. The effect of this fault could be realized by investigating equation (24). An increased slot area will result in a change of the mass flow rate and thus, the rate of cylinder pressure change that by inspecting equations (19) to (31), it is evident that will change the load torque that will be transferred to the electrical signals. This fault was simulated by a 50% increase in the slot area in this research. Lack of lubrication is also a common fault in the air compressors that is caused by a low level of oil or a fault in the compressor pump that will result in an increase in the friction coefficient of contact surfaces. The generated heat can harm the moving parts of the compressor. In this study, the lack of lubrication was simulated by increasing the friction coefficient by 200% that increases the frictional torque. The tank leakage fault often occurs at a very slow rate and is considered an isothermal process that will result in an exponential decay in the tank pressure [13]. This changes the effective pressure of the discharge plenum and changes the mass flow rate toward the discharge valve. This change contributes to the load torque by affecting the pressure change rate and thus, the force that the CV exerts on the piston. An increased piston-cylinder clearance is also simulated by leakage of the air from around the piston rings and also a changed friction coefficient. The effects of the simulated faults on the Fast Fourier Transform (FFT) of the current signal are shown in the results section.

IV. Apllication of ESA-Based Fault Diagnosis on the Experimental Setup

A. *Designing the experiment*

In order to implement the fault diagnosis of the compressor, an experimental setup was designed and data were acquired from the system. The studied compressor was a single-stage reciprocating compressor driven by a single-phase 2.5 hp induction motor that fills a 50 lit tank to a maximum pressure of almost 8 Bar. In this experiment, current, voltage, and pressure signals were acquired simultaneously from the setup with a sample rate of 8 kHz and were passed from a Chebyshev I anti-aliasing analog filter with a corner frequency of 3.7 kHz that was implemented on a supplementary board along with the electrical sensors and the power circuit. An overview of the experiment procedure and setup is shown in Fig. 3. Each time, the compressor filled the totally empty tank to the maximum pressure. This procedure was repeated 30 times for the healthy compressor and 10 times under the presence of each of the faults. A 0.75 mm hole in the discharge valve was inserted to simulate the valve leakage fault. The tank leakage fault was simulated by opening the tank discharge valve to let the air drain with an average flow of 22.4 $\frac{cm^3}{s}$. The piston-cylinder clearance was reduced by machining the piston rings to decrease their diameters by 0.5 mm and 20% of the compressor oil was drained to simulate the lack of lubrication fault.

B. *Signal Preprocessing and Feature Extraction*

After the data acquisition, the acquired signals were passed from a digital Butterworth filter with a corner frequency of 3 kHz. The phase shifts of the signals were then compensated and finally, a median filter was used to remove signal spikes.

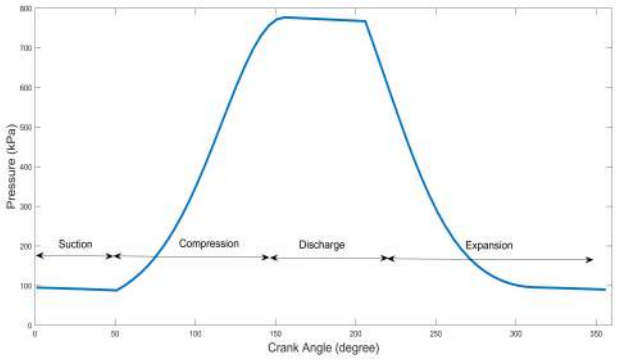

Fig. 2. Pressure calculated by mechanical sub-section model

After that, several time-domain and frequency-domain features were extracted from the signals. Signals were divided into segments that the pressure increased by 0.5 Bar in each of them, and the features were calculated for each segment. The calculated features included the time-domain energy, energy of each harmonic of the frequency domain, mean, variance, kurtosis, Root Mean Square (RMS), skewness, Signal to Noise Ratio (SNR), Total Harmonic Distortion (THD), and shape factor. Reducing the number of features can result in a simpler classifier, reduce the training time, and the possibility of overfitting [14]. Hence, the Pearson Correlation, Chi-squared, Recursive Feature Elimination, Lasso, and tree-based methods were used to indicate the most potent features and remove the less relevant ones. Among the features that these methods indicated as the most relevant ones, those that were selected by more than two methods were kept in the dataset. The results of the feature selection process are presented in the next sections.

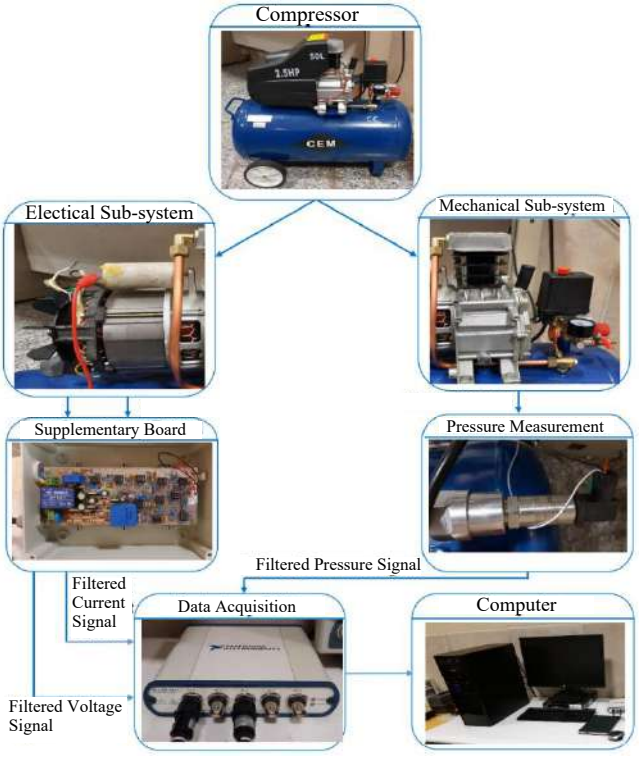

Fig. 3. An overall view of the experiment procedure and setup

C. Classification of Features

Classification of the extracted features was conducted using fine, medium, and coarse tree methods, the Naïve Bayes, SVM with linear and quadratic kernels, and fine and medium K-Nearest Neighbor (KNN) methods. The results obtained by using the linear SVM method were the most accurate and are presented in the next section as the results of the chosen method.

V. Results

In this section, numerical results of the simulation, feature selection and finally, condition classification are presented. The FFT of the current signal when valve leakage, lack of lubrication, tank leakage, and piston-cylinder clearance faults are added to the system are compared to the healthy system. The effects of introducing the faults are conspicuous in the peak values of the current FFT. The first and second peaks of the plot that represent the first and third harmonic of the FFT are magnified to provide a better view of the difference. The effect of introducing the valve leakage to the system is shown in Fig. 4. It can be seen that the first and second peak values of the current FFT, that represent the energy of the first and third harmonic of the current signal have reduced after introducing the fault. Reduction of the first two peak values in the current FFT also happens when the piston-cylinder clearance fault is introduced, as shown in Fig. 7. The lack of lubrication fault increases the frictional torque and thus, the load torque, which results in an increased total current. This effect is portrayed by the increased peak values in the first two peaks of the current FFT shown in Fig. 5. The subtlest effect among the studied faults is the slight decrease in the FFT peak values after introducing the tank leakage fault shown in Fig. 6. This is not counterintuitive since this fault only affects the mass flow rate toward the discharge valve.

The selected features that were chosen by voting among the employed feature selection methods and the number of methods that each selected feature gained are presented in Table 1. It can be deducted that the energy of different harmonics of voltage and current signals are the most suitable features to be used in the classification process. Another deduction that could be made from the table is that almost all of the selected features are the ones extracted from electrical signals and only one feature is selected from the features related to pressure. Despite the fact that the signal segmentation was implemented using pressure data, it was observed that by dividing the electrical signals into 15 equal segments and repeating the classification, the obtained accuracy did not deteriorate notably. On that account, the condition monitoring of the studied compressor could be performed by the mere utilization of electrical signals.

The confusion matrix of using the linear SVM algorithm is shown in Fig. 8. The matrix shown in the left side is obtained by using all features, whereas the right matrix shows the results of using only the selected features from the electrical signals. Evidently, the obtained accuracy has increased that ascertains the prosperity of the feature selection procedure. These results are calculated after performing five-fold cross validation. Using this approach, five models are trained using each of the methods, each time using 20% of the dataset as the validation set and 80% of it as the test set. Finally, an average of the five validation accuracies is reported as the accuracy of the model. This approach provides a suitable touchstone for evaluating the generalization ability of the method.

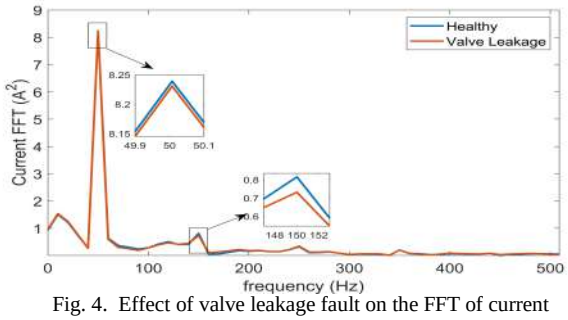

Fig. 4. Effect of valve leakage fault on the FFT of current

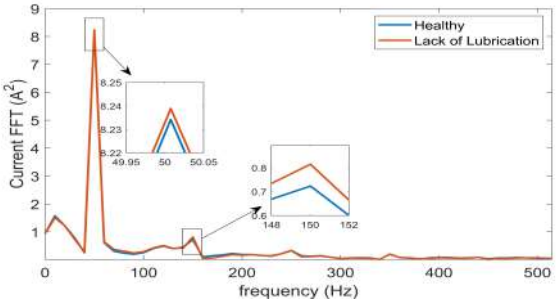

Fig. 5. Effect of lack of lubrication fault on the FFT of current

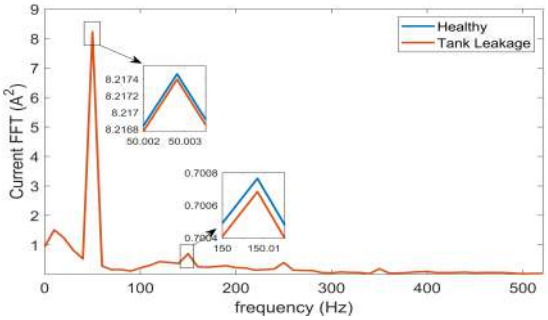

Fig. 6. Effect of tank leakage fault on the FFT of current

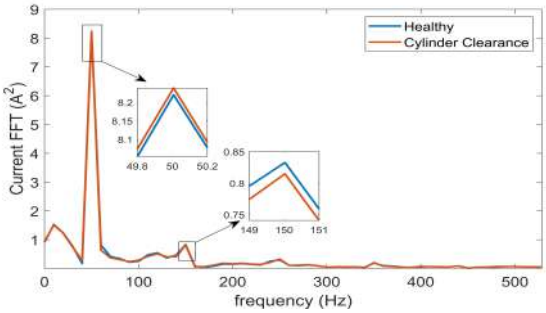

Fig. 7. Effect of piston-cylinder clearance fault on the FFT of current

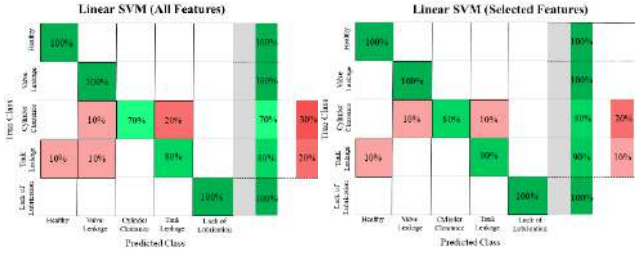

Fig. 8. Confusion matrices of the results obtained from the SVM method

VI. Conclusion

In this paper, the electromechanical coupling in an induction motor-driven reciprocating air compressor was studied and a fault detection approach based on electrical signature analysis was implemented. The set of ruling equations of the electrical and mechanical sub-systems was formed and using that, a simulation of the system was implemented. After introducing four types of mechanical faults to the system, their effects were shown on the FFT of the current signal. Afterward, data were acquired from an experimental setup and feature extraction, feature selection, and classification of the system condition were performed. Results showed that highly-accurate condition monitoring of the compressor could be accomplished using the electrical signature analysis and SVM method with linear kernel.

References

[1] J. Townsend, M. A. Badar, and J. Szekerces, "Updating temperature monitoring on reciprocating compressor connecting rods to improve reliability," *Eng. Sci. Technol. an Int. J.*, vol. 19, no. 1, pp. 566–573, 2016.

[2] K. Pichler, E. Lughofer, M. Pichler, T. Buchegger, E. P. Klement, and M. Huschenbett, "Fault detection in reciprocating compressor valves under varying load conditions," *Mech. Syst. Signal Process.*, vol. 70, pp. 104–119, 2016.

[3] P. Potočnik and E. Govekar, "Semi-supervised vibration-based classification and condition monitoring of compressors," *Mech. Syst. Signal Process.*, vol. 93, pp. 51–65, 2017.

[4] E. L. Bonaldi, L. E. de L. de Oliveira, J. G. B. da Silva, G. Lambert-Torresm, and L. E. B. da Silva, "Predictive maintenance by electrical signature analysis to induction motors," in *Induction Motors-Modelling and Control*, IntechOpen, 2012.

[5] P. Zhang and P. Neti, "Detection of gearbox bearing defects using electrical signature analysis for doubly fed wind generators," *IEEE Trans. Ind. Appl.*, vol. 51, no. 3, pp. 2195–2200, 2014.

[6] W. T. Thomson and M. Fenger, "Current signature analysis to detect induction motor faults," *IEEE Ind. Appl. Mag.*, vol. 7, no. 4, pp. 26–34, 2001.

[7] M. R. Shahriar, P. Borghesani, and A. C. C. Tan, "Electrical signature analysis-based detection of external bearing faults in electromechanical drivetrains," *IEEE Trans. Ind. Electron.*, vol. 65, no. 7, pp. 5941–5950, 2017.

[8] P. Popaleny, A. Duyar, C. Ozel, and Y. Erdogan, "Electrical Submersible Pumps Condition Monitoring Using Motor Current Signature Analysis," in *Abu Dhabi International Petroleum Exhibition & Conference*, 2018.

[9] F. Gu, Y. Shao, N. Hu, A. Naid, and A. D. Ball, "Electrical motor current signal analysis using a modified bispectrum for fault diagnosis of downstream mechanical equipment," *Mech. Syst. Signal Process.*, vol. 25, no. 1, pp. 360–372, 2011.

[10] A. E. Fitzgerald *et al.*, *Electric Machinery*, 6th ed. 2003.

[11] Z. Araste, M. J. Moghaddam, A. Toroghi, and A. Sadighi, "Study of-Electromechanical coupling in A Motor-Driven Centrifugal Pump for Fault Detection and Diagnosis," in *2019 7th International Conference on Robotics and Mechatronics (ICRoM)*, 2019, pp. 558–563.

[12] D. J. McCarthy, "Vibration-based diagnostics of reciprocating machinery." Massachusetts Institute of Technology, 1994.

[13] P. J. Pritchard and J. W. Mitchell, *Fox and McDonald's introduction to fluid mechanics*. John Wiley & Sons, 2016.

[14] M. H. Nguyen and F. De la Torre, "Optimal feature selection for support vector machines," *Pattern Recognit.*, vol. 43, no. 3, pp. 584–591, 2010.